

Activation of *Escherichia coli* UDP-3-*O*-[(*R*)-3-hydroxymyristoyl]-*N*-acetylglucosamine Deacetylase by Fe²⁺ Yields a More Efficient Enzyme with Altered Ligand Affinity[†]

Marcy Hernick,^{‡,⊥} Samuel G. Gattis,[§] James E. Penner-Hahn,^{‡,||} and Carol A. Fierke^{*,‡,§}

[‡]Department of Chemistry, [§]Department of Biological Chemistry, and ^{||}Department of Biophysics, University of Michigan, Ann Arbor, Michigan 48109. [⊥]Current address: Department of Biochemistry, Virginia Tech, Engel Hall, Blacksburg, VA 24061.

Received December 2, 2009; Revised Manuscript Received February 5, 2010

ABSTRACT: The metal-dependent deacetylase UDP-3-*O*-[(*R*)-3-hydroxymyristoyl]-*N*-acetylglucosamine deacetylase (LpxC) catalyzes the first committed step in lipid A biosynthesis, the hydrolysis of UDP-3-*O*-myristoyl-*N*-acetylglucosamine to form UDP-3-*O*-myristoylglucosamine and acetate. Consequently, LpxC is a target for the development of antibiotics, nearly all of which coordinate the active site metal ion. Here we examine the ability of Fe²⁺ to serve as a cofactor for wild-type *Escherichia coli* LpxC and a mutant enzyme (EcC63A), in which one of the ligands for the inhibitory metal binding site has been removed. LpxC exhibits higher activity (6–8-fold) with a single bound Fe²⁺ as the cofactor compared to Zn²⁺-LpxC; both metalloenzymes have a bell-shaped dependence on pH with similar pK_a values, indicating that at least two ionizations are important for maximal activity. X-ray absorption spectroscopy experiments suggest that the catalytic metal ion bound to Fe²⁺-EcLpxC is five-coordinate, suggesting that catalytic activity may correlate with coordination number. Furthermore, the ligand affinity of Fe²⁺-LpxC compared to the Zn²⁺ enzyme is altered by up to 6-fold. In contrast to Zn²⁺-LpxC, the activity of Fe²⁺-LpxC is redox-sensitive, and a time-dependent decrease in activity is observed under aerobic conditions. The LpxC activity of crude *E. coli* cell lysates is also aerobically sensitive, consistent with the presence of Fe²⁺-LpxC. These data indicate that EcLpxC can use either Fe²⁺ or Zn²⁺ to activate catalysis in vitro and possibly in vivo, which may allow LpxC to function in *E. coli* grown under different environmental conditions.

Treatment of infections caused by Gram-negative bacteria is often difficult, due in part to the antibiotic resistance associated with these organisms. Furthermore, Gram-negative organisms (e.g., *Yersinia pestis* and *Francisella tularensis*) have recently been identified as potential bioterror agents (1). For these reasons, new antibiotics that are effective in the treatment of Gram-negative bacterial infections are needed, including drugs that act on new targets. Possible targets in Gram-negative bacteria include the enzymes involved in the biosynthesis of lipopolysaccharides (LPS)¹ that make up the outer membranes of these

organisms (2–4). The lipid A portion of LPS is responsible for anchoring LPS to the cell surface; consequently, the lipid A biosynthetic pathway is a potential source of targets for antibiotic development (2). UDP-3-*O*-[(*R*)-3-hydroxymyristoyl]-*N*-acetylglucosamine deacetylase (LpxC) catalyzes the committed, and second overall, step in the biosynthesis of lipid A, the deacetylation of UDP-3-*O*-[(*R*)-3-hydroxymyristoyl]-*N*-acetylglucosamine to form UDP-3-*O*-[(*R*)-3-hydroxymyristoyl]glucosamine and acetate (Figure 1A) (5). Consequently, LpxC is an appealing target for antimicrobial development.

LpxC was originally classified as a “Zn²⁺-dependent” deacetylase on the basis of the findings that LpxC activity is reversibly inhibited by incubation with metal chelators [e.g., ethylenediaminetetraacetic acid (EDTA) and dipicolinic acid (DPA)] and LpxC is copurified with Zn²⁺ under aerobic conditions (6). However, these previous studies did not evaluate the ability of Fe²⁺ to activate LpxC. Recently, there have been several examples of Zn²⁺-dependent enzymes that have been reclassified as “Fe²⁺-dependent” enzymes, including peptide deformylase (PDF) (7–9), LuxS (10), and possibly histone deacetylase 8 (HDAC8) (11). The misidentification of the native metal cofactor as Zn²⁺ is attributed to the aerobic purification of these enzymes, with the oxidation of Fe²⁺ to Fe³⁺ and substitution of Zn²⁺ at the active site.

Herein, we demonstrate that replacement of the Zn²⁺ cofactor with Fe²⁺ in *Escherichia coli* LpxC both enhances the catalytic activity and alters the affinity of this enzyme for ligands. In fact, Fe²⁺-LpxC functions as a mononuclear metal-dependent

[†]This work was supported by the National Institutes of Health (Grant GM40602 to C.A.F. and Grant GM38047 to J.E.P.-H.) and the Cystic Fibrosis Foundation (Grant HERNIC05F0 to M.H.). S.G.G. was supported by National Institute of General Medical Sciences Training Grant F32 GM007767.

*To whom correspondence should be addressed. Phone: (734) 936-2678. Fax: (734) 647-4865. E-mail: fierke@umich.edu.

¹Abbreviations: LPS, lipopolysaccharide(s); LpxC, UDP-3-*O*-[(*R*)-3-hydroxymyristoyl]-*N*-acetylglucosamine deacetylase; EcLpxC, *Escherichia coli* LpxC; AaLpxC, *Aquifex aeolicus* LpxC; EDTA, ethylenediaminetetraacetic acid; DPA, dipicolinic acid; UDP-GlcNAc, uridine-5'-diphosphate *N*-acetylglucosamine; myr-UDP-GlcNAc, UDP-3-*O*-[(*R*)-3-hydroxymyristoyl]-*N*-acetylglucosamine; myr-UDP-GlcNH₂, UDP-3-*O*-[(*R*)-3-hydroxymyristoyl]glucosamine; PDF, peptide deformylase; HDAC, histone deacetylase; XAS, X-ray absorption spectroscopy; EXAFS, extended X-ray absorption fine structure; XANES, X-ray absorption near-edge structure; ICP-MS, inductively coupled plasma emission spectroscopy-mass spectrometry; WT, wild type; BSA, bovine serum albumin; TCEP, tris(carboxyethyl)phosphine; DTT, dithiothreitol; DMSO, dimethyl sulfoxide; MWCO, molecular weight cutoff; BODIPY 500/510 C₄, C₉, 5-butyl-4,4-difluoro-4-bora-3a,4a-diaza-s-indacene-3-nonanoic acid; PDB, Protein Data Bank.

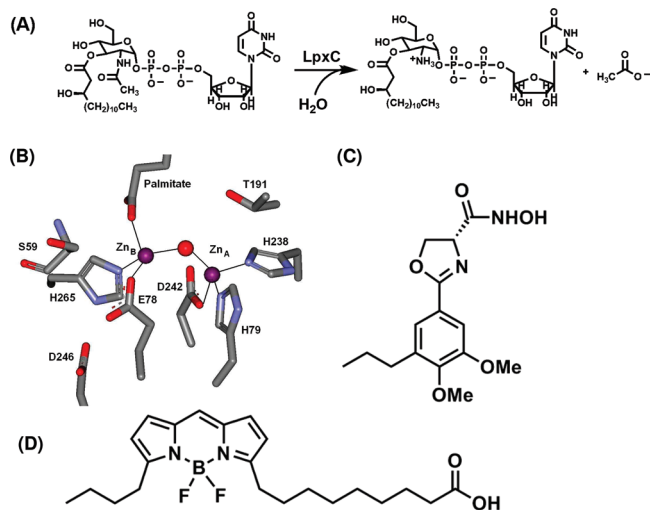


FIGURE 1: (A) LpxC-catalyzed reaction. (B) Active site of LpxC from *Aquifex aeolicus* containing two zinc ions: Zn_A (catalytic) and Zn_B (inhibitory). This figure was made from PDB entry 1P42. (C) Structure of L-161,240. (D) Structure of BODIPY-fatty acid.

deacetylase with a catalytic activity that is ~ 6 -fold higher than that of Zn^{2+} -LpxC. This enhancement in catalytic activity is due primarily to an increase in the value of the parameter k_{cat} , not K_M . X-ray absorption spectroscopy (XAS) experiments indicate that the metal ion in Fe^{2+} -LpxC is five-coordinate, suggesting that higher coordination numbers correlate with enhanced catalytic activity. In contrast to Zn^{2+} -LpxC, the activity of the Fe^{2+} -bound enzyme is sensitive to oxygen. Furthermore, the activity of native LpxC in crude *E. coli* cell lysates is aerobically sensitive, consistent with the presence of Fe^{2+} -LpxC. These findings suggest that under normal growth conditions the native metal bound to LpxC in *E. coli* is Fe^{2+} . However, it is possible that the active site metal bound to LpxC in vivo could switch depending on the metal ion availability, thus allowing LpxC to function using different metal ion cofactors under different environmental conditions.

MATERIALS AND METHODS

General Procedures. *E. coli* (WT and C63A variant) and *A. aeolicus* LpxC (AaLpxC) were overexpressed and purified according to published procedures using DEAE-Sepharose and Reactive Red-120 affinity dye columns at 4 °C and room temperature, respectively (5, 6, 12, 13). The apo and single-metal-bound forms of LpxC were prepared by treatment with metal chelators (DPA and EDTA) followed by reconstitution with Zn^{2+} or Fe^{2+} , as previously described (6, 14). All solutions (except for enzyme) were degassed with Ar prior to use. For Fe^{2+} experiments, a 400 mM $FeCl_2$ stock was prepared in 10 mM dithionite and diluted to 100 μ M with 1 \times assay buffer prior to incubation with apo-LpxC. Similarly, a 100 mM $ZnSO_4$ solution was prepared in 25 mM bis-tris propane and 1.5 mM triscarboxyethylphosphine (TCEP) (pH 7.5–8.7) and diluted to 100 μ M with 1 \times assay buffer prior to incubation with apo-LpxC. The concentrations of metal stocks were verified by ICP-MS. To maintain anaerobic conditions, experiments were conducted either in an anaerobic chamber (Coy Laboratory Products, Grass Lake, MI) or using assay buffers containing 10 mM TCEP and were completed in <2 h to ensure that LpxC was maximally active during the course of the assays. All ICP-MS analysis was conducted at the University of Michigan, Department of Geology, by T. Huston.

LpxC Deacetylase Assay. [^{14}C]UDP-3-*O*-(3-hydroxymyristoyl)-*N*-acetylglucosamine was prepared, and the deacetylase activity was measured as previously described (6, 14, 15). To examine the metal ion stoichiometry of the Zn^{2+} -LpxC-catalyzed reactions, apo-LpxC was incubated [5 μ M WT or C63A in 20 mM bis-tris propane (pH 7.5)] with 0–2 equiv of $ZnSO_4$ for 1–2 h at room temperature to allow for holoenzyme formation and was then diluted to 100–200 nM in assay buffer just prior to activity measurement. For the Fe^{2+} stoichiometry, apo-LpxC [10 μ M WT or C63A in 20 mM bis-tris propane and 2–10 mM TCEP (pH 7.5)] was incubated with $FeCl_2$ (1 to 500 μ M) on ice for 5–60 min in an anaerobic chamber (at <10 mM TCEP) and then diluted with assay buffer prior to the measurement of activity. Assay mixtures containing 20 mM bis-tris propane (pH 7.5), 10 mM TCEP (for Fe^{2+} measurements), bovine serum albumin (BSA, fatty acid free, 1 mg/mL), and [^{14}C]UDP-3-*O*-(3-hydroxymyristoyl)-*N*-acetylglucosamine (0.05–4 μ M) were pre-equilibrated at 30 °C, and the reactions were initiated by the addition of enzyme (from 0.5 to 5 nM). ICP-MS results indicate these samples contain ≤ 20 nM zinc. After incubation for various times, the reactions were quenched by the addition of sodium hydroxide, which also cleaves the myristate substituent from substrate and product for ease of separation. Substrate and product were separated on PEI-cellulose TLC plates (0.1 M guanidinium HCl) and quantified by scintillation counting, and the initial rates of product formation (<20% reaction) were determined from these data. To evaluate the steady-state kinetic parameters, activity was measured at seven to nine different concentrations of myr-UDP-GlcNAc (from 50 nM to 4 μ M). The steady-state parameters k_{cat} , K_M , and k_{cat}/K_M were obtained by fitting the Michaelis–Menten equation to the initial linear velocities measured at the various substrate concentrations using the curve fitting program Kaleidagraph (Synergy Software), which also calculates the asymptotic standard errors. For pH studies of C63A LpxC, 20 mM bis-tris (pH 5.7–6.5) or bis-tris propane (pH 7–10) with 10 mM TCEP was used and pK_a values were obtained by fitting eq 1 to these data. Control experiments demonstrate that incubation of LpxC at various pH values for up to 30 min does not lead to an irreversible decrease in activity.

For experiments with the hydroxamate inhibitor L-161,240 (13, 16, 17), a generous gift from M. Pirrung, Zn^{2+} - or Fe^{2+} -LpxC (0.5 nM) was preincubated with inhibitor (from 0.5 to 500 nM, DMSO) or DMSO for 15–25 min at 30 °C in 20 mM bis-tris propane, 10 mM TCEP (pH 7.5), and 1 mg/mL BSA prior to initiation of the reaction by the addition of [^{14}C]UDP-3-*O*-(3-hydroxymyristoyl)-*N*-acetylglucosamine (200 nM). Initial rates were processed as described above, and the IC_{50} values were obtained by fitting eq 2 to these data.

$$\frac{V}{k_{obs}} = \frac{k_1}{1 + \frac{[H^+]}{K_{a1}} + \frac{K_{a2}^2}{[H^+]^2}} \quad (1)$$

$$v = \frac{IC_{50}}{[I] + IC_{50}} \quad (2)$$

Ultrafiltration Binding Assay. Dissociation constants (K_D) of [^{14}C]UDP-3-*O*-(3-hydroxymyristoyl)glucosamine from LpxC·product complexes were measured using ultrafiltration, as previously described (18). Briefly, the concentration of product was held constant (50–60 nM) and the concentration of wild-type or

C63A LpxC was varied (from 0 to 24 μM). Enzyme and substrate were incubated at 30 °C for 15–30 min prior to the assay to allow for product formation and ligand equilibration. Assay mixtures were then transferred into ultrafiltration devices (Microcon 30000 MWCO), and the free and bound products were separated by centrifugation of the samples at 3000 rpm for 2.5 min. Equal volumes of the filtrate and retentate were removed, and the amounts of unbound (filtrate) and total product (retentate) were quantified using scintillation counting. The $\text{EP}/P_{\text{total}}$ ratio was determined as a function of E_{total} , and the K_{D} values were obtained by fitting eq 3 to these data.

$$\frac{\text{EP}}{P_{\text{total}}} = \frac{\left(\frac{\text{EP}}{P_{\text{total}}}\right)_{\text{Endpt}}}{1 + \frac{K_{\text{D}}}{E_{\text{total}}}} + \left(\frac{\text{EP}}{P_{\text{total}}}\right)_{\text{Bkgd}} \quad (3)$$

K_{D} fatty acid Determination Using Fluorescence Anisotropy Measurements. The K_{D} value of 5-butyl-4,4-difluoro-4-bora-3a,4a-diaza-s-indacene-3-nonanoic acid [BODIPY 500/510 C₄, C₉ (Invitrogen)] fatty acid for EcLpxC was determined using fluorescence anisotropy as previously described (18, 19). The concentration of BODIPY fatty acid was held constant (0.1 μM) [in 25 mM HEPES, 10 mM TCEP (pH 7.5), and 100 μM FeCl_2], and increasing concentrations of enzyme (from 0 to 100 μM) were titrated into the solution at 30 °C. The fluorescence anisotropy (excitation at 480 nm and emission at 516 nm) was measured ~3 min after each addition of LpxC, and K_{D} values were determined by fitting eq 4 to these data.

$$\frac{E \cdot \text{FA}}{\text{FA}_{\text{total}}} = \frac{\left(\frac{E \cdot \text{FA}}{\text{FA}_{\text{total}}}\right)_{\text{Endpt}}}{1 + \frac{K_{\text{D}}}{E_{\text{total}}}} + \text{FL}_{\text{Bkgd}} \quad (4)$$

X-ray Absorption Spectroscopy. XAS samples were prepared and analyzed as previously described (12). Briefly, a stoichiometric amount of apo-EcLpxC or apo-AaLpxC was added to a solution of 24 μM FeCl_2 (anaerobic chamber) or ZnSO_4 in 25 mM HEPES and 1.5 mM TCEP (pH 7.5) and incubated on ice for 45 min (AaLpxC, room temperature for 25 min). The enzyme was concentrated using an Amicon Ultra-15 centrifugal filter unit (10000 MWCO), and unbound metal ions were removed by washing with buffer [25 mM HEPES, 1.5 mM TCEP (pH 7.5)] prior to concentration. Glycerol (20 μL) was mixed with the enzyme (60 μL) as a cryoprotectant, and samples were transferred into Lucite cuvettes (3 mm \times 2 mm \times 25 mm) with 40 μm Kapton windows and frozen in liquid N_2 . The concentrations of Fe, Co, and Zn were determined using ICP-MS, and all analyzed samples had a metal/enzyme stoichiometry of <1 (range of 0.14–0.63). XAS data were collected at the Stanford Synchrotron Radiation Laboratory (beamline 9-3) under dedicated conditions as fluorescence excitation spectra, using a solid-state Ge detector array equipped with a filter and Soller slits focused on the sample. All channels of each scan were examined for glitches, and the good channels were averaged for each sample (two independent samples for each protein) to give the final spectrum.

EXAFSPAK (20) was used to extract and analyze EXAFS data as previously described (12), using ab initio phase and amplitude parameters calculated using FEFF version 7.02 (21, 22). XANES data were normalized to tabulated absorption coefficients (23) using MBACK (24). The area of the 1s \rightarrow 3d transition

in the XANES region was calculated by fitting the pre-edge region (7107–7118 eV) using the sum of a Gaussian and an arctan function; for comparison with previously published data, the fitted Gaussian area was normalized to the K-edge jump for Fe ($3.556 \times 10^2 \text{ cm}^2/\text{g}$).

Native LpxC Deacetylase Activity. LB medium was inoculated with BL21(DE3) or BL21(DE3)pLysS cells and grown in a shaker (250 rpm) overnight at 37 °C. The cells were harvested by centrifugation and the cell pellets resuspended in 20 mM bis-tris propane, 0–10 mM TCEP (pH 7.5). The cells were washed with 5 mM CaCl_2 ($1 \times 2 \text{ mL}$) followed by buffer ($2 \times 2 \text{ mL}$), resuspended in buffer, and stored at -80 °C. Control experiments demonstrate that Ca^{2+} ($\leq 10 \text{ mM}$) has no significant effect on Zn^{2+} -LpxC activity. Prior to the assay of activity, cells were thawed and incubated with lysozyme (0.2–1.2 mg/mL) in assay buffer for 15 min at room temperature and the cell lysate was cleared by centrifugation (14000 rpm for 15 min). A sample of the cleared lysate was analyzed for metal content by ICP-MS; the concentration of total Fe in these lysates is ~2-fold greater than that of Zn (Fe/Zn ratio of 1.4–3.0). The cleared lysate was diluted 10-fold in assay buffer prior to measurement of activity as described above (200 nM substrate). To demonstrate that the observed activity was catalyzed by LpxC, the activity was also measured in the presence of the inhibitor L-161,240. In vitro control experiments indicate that exchange of Zn^{2+} for Fe^{2+} is facile in vitro, but the opposite metal exchange is not readily observed and is likely thermodynamically unfavorable (25). Therefore, the experiments in cell lysates should err on the side of underestimating the concentration of Fe^{2+} -LpxC.

RESULTS

The Activity of Fe^{2+} -LpxC Is Higher Than That of Zn^{2+} -LpxC. Activation of apo-LpxC by various divalent metal ions was previously demonstrated with the ions in the following order: $\text{Co}^{2+} > \text{Zn}^{2+} > \text{Ni}^{2+} > \text{Mn}^{2+}$. No increase in activity was observed following the addition of Mg^{2+} , Ca^{2+} , Cd^{2+} , or Cu^{2+} to apo-LpxC (6). Stoichiometric addition of Zn^{2+} and Co^{2+} fully activates apo-LpxC, while an excess concentration of Ni^{2+} (~3:1 Ni^{2+} :LpxC ratio) is required, suggesting that LpxC has weaker affinity for Ni^{2+} (6). On the basis of these findings and the fact that aerobically purified LpxC contains one to three Zn^{2+} ions per enzyme, LpxC was characterized as a “zinc-dependent” deacetylase (6). Here we probe whether Fe^{2+} can also activate apo-LpxC.

Since Fe^{2+} is a redox-sensitive metal ion, activation of LpxC by Fe^{2+} was measured under anaerobic conditions (glovebox or 10 mM TCEP). Under these conditions, addition of Fe^{2+} (1–3 equiv) activates apo-LpxC. In fact, the initial velocity for deacetylation of myr-UDP-GlcNAc (0.2 μM) under standard assay conditions (pH 7.5) is 6–9-fold higher with Fe^{2+} -LpxC than with Zn^{2+} -LpxC, indicating that Fe^{2+} , like Co^{2+} , is better suited than Zn^{2+} at enhancing the catalytic activity of LpxC. Furthermore, comparable activity is observed for LpxC in the presence of both 1 and 3 equiv of Fe^{2+} , suggesting that the enzyme is saturated with Fe^{2+} under the preincubation conditions.

Metal Ion Stoichiometry. Crystal structures of AaLpxC reveal that the LpxC active site contains two metal ion binding sites [Figure 1B, (26)]: one catalytic site, Zn_A , and one inhibitory site, Zn_B . EcLpxC is activated by stoichiometric addition of either Zn^{2+} or Co^{2+} , while the addition of excess Zn^{2+} inhibits enzyme activity (6). Similarly, the activity of apo-EcLpxC is

activated by the addition of Fe^{2+} . For WT LpxC, an initial increase in LpxC activity is observed as the concentration of metal is increased from zero to one metal ion per enzyme for both Fe^{2+} and Zn^{2+} , followed by a decrease in enzyme activity as the concentration of metal ion is increased further (Figure 2), although the inhibition by zinc is significantly more severe. These results are consistent with metal ion binding tightly at the catalytic site to enhance catalytic activity, followed by binding of a weaker, second metal ion at the inhibitory site that decreases the observed catalytic activity. Comparison of the maximal activities achieved with Fe^{2+} and Zn^{2+} suggests that LpxC is 6–9-fold more active with bound Fe^{2+} than Zn^{2+} ; however, direct comparison of these activities in the WT enzyme is complicated by metal ion binding at the inhibitory site.

C63A Mutation in LpxC Decreases the Level of Metal Ion Inhibition. To circumvent complications arising from metal ion inhibition, we proposed to preferentially decrease the metal affinity of the inhibitory site by selectively removing a ligand from this site. Structural data for AaLpxC indicate that the ligands for the inhibitory Zn^{2+} ion are the side chains of E78 and H265, a bound palmitate, and the catalytic water molecule [Figure 1B (26)], while EXAFS experiments indicate that the inhibitory Zn^{2+} in EcLpxC has at least one S/Cl ligand (12). Sequence alignment of EcLpxC with AaLpxC and mapping of the Cys side chains onto the AaLpxC structure indicated that the side chain of Cys63 [equivalent to Ser59 in AaLpxC (Figure 1B)] is the only S atom within 10 Å of the inhibitory Zn^{2+} ion, implying that Cys63 is the third protein ligand for the inhibitory

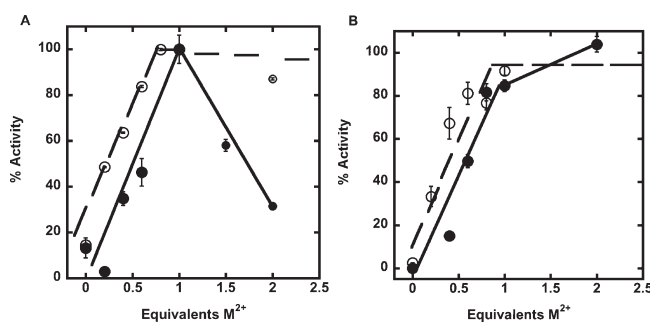


FIGURE 2: Activation of apo-LpxC by Zn^{2+} or Fe^{2+} . Deacetylase activity as a function of either Zn^{2+} (●) or Fe^{2+} (○) metal ion stoichiometry was measured for WT LpxC (A) and C63A LpxC (B). C63A LpxC activity was assayed with an up to 50-fold excess Fe^{2+} (not shown). The deacetylase activity for the substrate myr-UDP-GlcNAc (0.2 μM) was measured at 30 °C after incubation with varying equivalents of M^{2+} , as described in Materials and Methods.

metal ion site in EcLpxC (18, 19). Since the side chains of E78 and H265 play important roles in the catalytic mechanism of LpxC (14, 27), we chose to prepare the EcC63A mutant to further compare the properties of Zn^{2+} and Fe^{2+} -LpxC.

Stoichiometric addition of either Fe^{2+} or Zn^{2+} to C63A LpxC increases the catalytic activity to $\geq 80\%$ of the maximal value observed at higher metal concentrations, indicating that C63A LpxC is activated by a single Fe^{2+} or Zn^{2+} ion. Furthermore, the level of inhibition of C63A LpxC by metal ions is significantly reduced, consistent with the Cys63 side chain serving as a ligand for the inhibitory metal ion binding site. This decrease in the level of metal ion inhibition facilitates a more accurate comparison of the maximal LpxC activity with the Fe^{2+} and Zn^{2+} cofactors.

Fe^{2+} Activates Steady-State Turnover. Steady-state turnover was measured for LpxC (WT and C63A) reconstituted with stoichiometric Fe^{2+} or Zn^{2+} (Table 1), demonstrating that the value of $k_{\text{cat}}/K_{\text{M}}$ for LpxC reconstituted with Fe^{2+} compared to that with Zn^{2+} is enhanced 8-fold. The C63A mutation also increases the value of $k_{\text{cat}}/K_{\text{M}}$ for LpxC reconstituted with Zn^{2+} and Fe^{2+} by 5- and 3.5-fold, respectively, relative to that of the wild-type enzyme, at least partly due to a decreased level of metal inhibition. Since the data obtained for WT LpxC are complicated by differences in metal ion inhibition, we measured the relative effects of Zn^{2+} and Fe^{2+} on the steady-state parameters for the C63A mutant. These results (Table 1 and Figure 3) show that switching the metal ion cofactor in C63A LpxC from Zn^{2+} to Fe^{2+} increases the values of both k_{cat} (4-fold) and $k_{\text{cat}}/K_{\text{M}}$ (6-fold) with little effect on the value of K_{M} .

The WT LpxC-catalyzed reaction exhibits a bell-shaped dependence on pH, where $\text{pK}_{\text{a}1}$ and $\text{pK}_{\text{a}2}$ are proposed to represent ionization of Glu78 and another group located near the metal ion, such as H265, respectively (14, 27). The pH dependence of $k_{\text{cat}}/K_{\text{M}}$ catalyzed by C63A LpxC activated by Zn^{2+} or Fe^{2+} (Figure 4) shows a bell-shaped pH profile, indicating that at least two ionizations are important for maximal activity, consistent with pH profiles previously measured for WT LpxC (14, 27). However, at high pH, the decrease in activity for C63A LpxC has a squared dependence on the proton concentration (Figure 4), suggesting that two deprotonations affect the activity at high pH. Therefore, the C63A mutant is best described by three ionizations: one at low pH and two at high pH. These data are fit using an equation that assumes that the two high-pH ionizations have comparable pK_{a} values. The reactions catalyzed by EcC63A LpxC reconstituted with a stoichiometric amount of either Zn^{2+} or Fe^{2+} have nearly identical pH profiles, indicating that the Fe-bound enzyme has higher catalytic activity regardless

Table 1: Steady-State Activity Parameters for EcLpxC

enzyme ^a	k_{cat}^b (min^{-1})	K_{M}^b (μM)	$k_{\text{cat}}/K_{\text{M}}^b$ ($\text{min}^{-1} \mu\text{M}^{-1}$)	$\text{pK}_{\text{a}1}^c$	$\text{pK}_{\text{a}2}^c$	$k_{\text{cat}}/K_{\text{M}}$ ($\text{min}^{-1} \mu\text{M}^{-1}$) at pH maximum ^c
Zn^{2+} -LpxC ^d	not determined	not determined	34 ± 8^d	6.2 ± 0.2^e	9.2 ± 0.2^e	not determined
Fe^{2+} -LpxC	90 ± 3	0.32 ± 0.04	281 ± 24	not determined	not determined	not determined
Zn^{2+} -C63A	126 ± 12	0.7 ± 0.2	170 ± 34	6.6 ± 0.1	8.9 ± 0.1	260 ± 20
Fe^{2+} -C63A	530 ± 30	0.5 ± 0.1	990 ± 130	6.8 ± 0.1	9.2 ± 0.1	760 ± 20

^aLpxC was reconstituted with stoichiometric (1:1) metal in a preincubation step, as described in Materials and Methods. The measured values for $k_{\text{cat}}/K_{\text{M}}$ catalyzed by apo-LpxC and apo-C63A LpxC are 15 and $11 \text{ min}^{-1} \mu\text{M}^{-1}$, respectively, likely due to metal contamination in the assay. ^bThe initial rates of LpxC deacetylase activity were determined at 30 °C [20 mM bis-tris propane, 10 mM TCEP (pH 7.5), and 1 mg/mL BSA] with myr-UDP-GlcNAc as the substrate as described in Materials and Methods. The kinetic parameters were obtained by fitting the Michaelis–Menten equation to the initial velocities. ^cDeacetylation of myr-UDP-GlcNAc catalyzed by LpxC (Fe^{2+} -WT and C63A) was assessed at 30 °C as a function of pH using substrate concentrations below the K_{M} (<0.2 μM). The pK_{a} values were obtained from the pH dependence of the values using eq 1 as described in Materials and Methods. ^d $k_{\text{cat}}/K_{\text{M}}$ for WT ZnLpxC is reported as the mean and standard deviation of five replicates performed at a single subsaturating substrate concentration (200 nM) with LpxC incubated with a stoichiometric amount of Zn^{2+} . ^eTaken from ref 14.

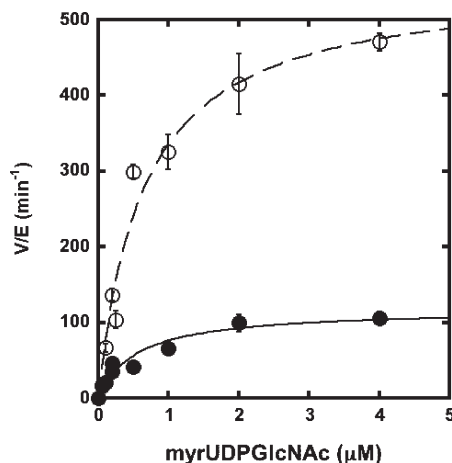


FIGURE 3: Steady-state turnover catalyzed by EcC63A substituted with Zn^{2+} (●) or Fe^{2+} (○). The initial rates for deacetylation of myr-UDP-GlcNAc ($0.05\text{--}4\text{ }\mu\text{M}$) were measured at $30\text{ }^{\circ}\text{C}$ in 20 mM bis-tris propane and 10 mM TCEP (pH 7.5), as described in Materials and Methods using apoenzyme reconstituted with stoichiometric metal ion. The parameters k_{cat} , K_{M} , and $k_{\text{cat}}/K_{\text{M}}$ (Table 1) were obtained by fitting the Michaelis–Menten equation to these data.

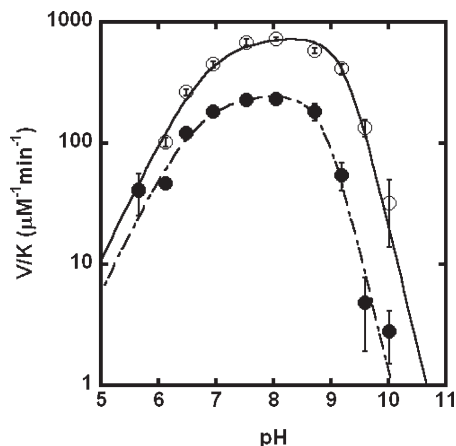


FIGURE 4: pH dependence of the LpxC-catalyzed deacetylase activity for C63A Zn^{2+} -LpxC (●) or C63A Fe^{2+} -LpxC (○). The values of V/K were measured at $30\text{ }^{\circ}\text{C}$ using subsaturating concentrations of myr-UDP-GlcNAc ($\leq 0.2\text{ }\mu\text{M}$) and enzyme reconstituted with stoichiometric metal ion, as described in Materials and Methods. The pK_{a} values (see Table 1) were determined by fitting eq 1 to the data.

of the pH. Furthermore, the fitted values for $\text{pK}_{\text{a}1}$ and $\text{pK}_{\text{a}2}$ for the C63A mutant are slightly higher than and comparable to, respectively, the values determined for WT LpxC, suggesting that the same ionizations are observed for both WT and the C63A mutant. The additional ionization at high pH observed for the C63A mutant could be due to several factors. For example, several ionizable LpxC residues not directly implicated in catalysis, such as H19 or K143 (18), could be perturbed in the C63A mutant, and ionization of these residues could become observable in the steady-state kinetics. Alternatively, replacing the cysteine thiol with an alanine may lower the metal–water pK_{a} such that it is observable at high pH. Ionization of these groups could directly affect the stability of the transition state or could reversibly destabilize the active structure of LpxC.

XAS Analysis of LpxC. The change in LpxC activity observed with Fe^{2+} and Zn^{2+} cofactors may correlate with an alteration in the preferred coordination numbers and/or geometries of the respective metal ions. For peptide deformylase (PDF),

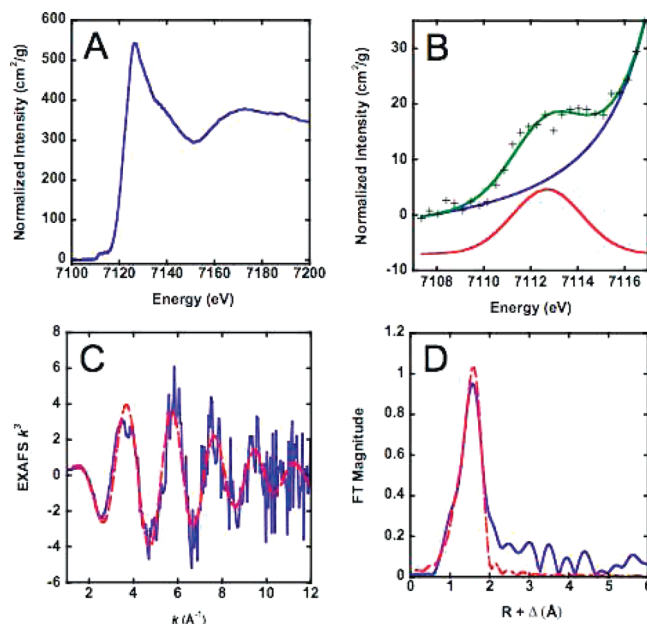


FIGURE 5: XAS of Fe^{2+} -EcLpxC. (A) XANES region. (B) Expansion of XANES showing the $1s \rightarrow 3d$ transition with a calculated background (blue) and best fit (green). The Gaussian fit to the $1s \rightarrow 3d$ transition is shown offset vertically for the sake of clarity. (C) k^3 -weighted EXAFS data (blue) together with the best fit using five oxygen ligands (red, dashed). (D) Fourier transform of EXAFS data: experimental (solid line) and fit (dashed line) to five N or O ligands.

the higher coordination number of Fe^{2+} -PDF compared to that of Zn^{2+} -PDF is proposed to contribute to the higher activity that is observed with the Fe^{2+} cofactor (28). In biological zinc sites, a coordination number of four (tetrahedral geometry) is observed most frequently, although five and six ligands are also observed, while Fe^{2+} prefers higher coordination numbers (five or six) (29–31). Previous XAS studies of AaLpxC and *Pseudomonas aeruginosa* LpxC (PaLpxC) with a single bound Zn^{2+} (12) demonstrated that the catalytic zinc ion has four N or O ligands. Similarly, crystal structures of the zinc-inhibited form and the cacodylate complex of AaLpxC indicate that the catalytic zinc ion is tetrahedral (26, 32). The best fits to the EXAFS data for EcLpxC with Zn^{2+} bound to both the catalytic and inhibitory sites include three N or O atoms and one S or Cl atom, while the fit for EcLpxC with Co^{2+} at the catalytic site includes five N or O atoms. These previously published data suggest that the increased activity of Co^{2+} -EcLpxC (17) correlates with the higher coordination number.

To probe determinants of the enhanced activity of Fe^{2+} -LpxC, we examined the coordination environments of EcLpxC and AaLpxC with a stoichiometric amount of Fe^{2+} bound at the catalytic site. The XANES and EXAFS data for these samples are shown in Figure 5. The XANES region of the XAS spectra ($1s \rightarrow 3d$ transitions) provides valuable information about metal ion coordination number and oxidation state. The $1s \rightarrow 3d$ transitions (pre-edge areas) observed for four-, five-, and six-coordinate Fe are $19.8\text{--}25 \times 10^{-2}$, $12.4\text{--}18.8 \times 10^{-2}$, and $3.1\text{--}9.9 \times 10^{-2}\text{ eV}$, respectively (33–35). The Fe pre-edge areas calculated for EcLpxC ($12.1 \times 10^{-2}\text{ eV}$) and AaLpxC ($11.2\text{--}14.9 \times 10^{-2}\text{ eV}$) are both consistent with a five-coordinate Fe species (Table 2) and, in particular, are significantly smaller than the values observed for tetrahedral Fe. This conclusion is supported by the EXAFS data for both WT Fe^{2+} -EcLpxC and Fe^{2+} -AaLpxC (Table 3 and Figure 5). Consistent with our

Table 2: XANES Pre-Edge Areas

sample	1s → 3d (sample 1)	1s → 3d (sample 2)	1s → 3d average
Fe ²⁺ -AaLpxC	11.2 × 10 ⁻² eV	14.9 × 10 ⁻² eV	13.1 × 10 ⁻² eV
Fe ²⁺ -EcLpxC	12.1 × 10 ⁻² eV	12.1 × 10 ⁻² eV	12.1 × 10 ⁻² eV

Table 3: Fitting Results for Fe-LpxC

	N^a	$R\text{ (\AA)}^b$	$\sigma^2\text{ (}\times 10^3\text{ \AA}^2\text{)}$	F^c	BVS^d
Fe ²⁺ -AaLpxC					
sample 1	4	2.100	5.7	0.66	1.5
	5	2.100	7.7	0.67	1.9
	6	2.100	9.7	0.70	2.2
sample 2	4	2.100	6.0	0.40	1.5
	5	2.096	8.2	0.42	1.9
	6	2.097	10.5	0.44	2.3
Fe ²⁺ -EcLpxC					
sample 1	4	2.100	6.4	0.30	1.5
	5	2.105	8.2	0.30	1.8
	6	2.106	10.1	0.32	2.2
sample 2	4	2.090	6.8	0.33	1.5
	5	2.090	8.8	0.33	1.9
	6	2.090	10.9	0.35	2.3

^aEXAFS coordination number, fixed at integer values. ^bFe–O bond length. Although the experimental accuracy is estimated to be ±0.02 Å, values are reported to 0.001 Å to show the precision of the data. ^cRoot-mean-square deviation between data and fit. ^dBond-valence sum.

observations for Zn-AaLpxC and Zn-PaLpxC (12), the EXAFS data for Fe²⁺-EcLpxC and Fe²⁺-AaLpxC show significant disorder. Fits using four, five, or six low-*Z* ligands all give similar quality fits, with Debye–Waller factors that increase as the fitted coordination number increases (Table 3). Although it was possible in most cases to fit the data using a mixed ligation mode of three to five O or N atoms and one S atom, in no case did these fits result in a more than modest (i.e., < 10%) improvement in fit quality, improvement that can be ascribed to the doubling in the number of adjustable parameters. Further evidence that the EXAFS data do not support the presence of mixed (N/O)+S ligation comes from the fact that in most cases the apparent Fe–S parameters were chemically unreasonable (e.g., apparent Fe–S distances of < 2 Å and apparent Fe–S Debye–Waller factors *σ*² of > 0.01 Å²). In all cases, both N/O only and (N/O)+S fits, the apparent Fe–(N/O) distance was ~2.1 Å, significantly longer than that found for the four-coordinate Zn²⁺ that is observed in many XAS and crystallographic studies of AaLpxC, PaLpxC, and EcLpxC (12), and consistent with the distances found for five-coordinate Fe²⁺. This conclusion is supported by the fact that the five-coordinate Fe–(N/O) fits consistently give the bond-valence sum values (36, 37) closest to 2.

Crystallographic analyses of AaLpxC and PaLpxC in complexes with hydroxamate inhibitors or palmitate indicate that the catalytic zinc changes geometry upon ligand binding to square pyramidal (five-coordinate) (26, 38). These data indicate that the geometry of the metal site is flexible, consistent with our finding that the Fe²⁺ site appears to adopt a five-coordinate structure even in the absence of added inhibitors. Since the Fe-LpxC coordination sphere is best fit to five N or O ligands, the added ligand is most likely a water molecule as observed in other proteins where metal substitution leads to a higher coordination number, such as carbonic anhydrase (39) and peptide deformylase (28). These observations are consistent with the suggestion

Table 4: LpxC Molecular Recognition Parameters

enzyme ^a	<i>K</i> _D ^{product} (μM) ^b	<i>K</i> _D ^{fatty acid} (μM) ^c	IC ₅₀ (nM) ^d
apo-LpxC	1.5 ± 0.5	25 ± 1	not determined
Zn ²⁺ -LpxC	1.6 ± 0.2 ^e	7 ± 0.6 ^f	not determined
Fe ²⁺ -LpxC	1.9 ± 0.3	45 ± 3	not determined
apo-C63A	0.5 ± 0.1	17 ± 1	not determined
Zn ²⁺ -C63A	0.40 ± 0.07	7 ± 1	4 ± 0.4
Fe ²⁺ -C63A	0.6 ± 0.1	44 ± 3	2 ± 0.2

^aMetal-substituted LpxC was reconstituted with stoichiometric metal ion (1:1) as described in Materials and Methods. ^bProduct (myr-UDP-GlcNH₂) binding to LpxC was assessed at 30 °C [20 mM bis-tris propane, 10 mM TCEP (pH 7.5)] using ultrafiltration as described in Materials and Methods. The *K*_D values were obtained by fitting eq 3 to the data. ^cBODIPY-fatty acid binding to LpxC was assessed at 30 °C [20 mM bis-tris propane, 10 mM TCEP (pH 7.5), and 100 μM ZnSO₄ or FeCl₂] using fluorescence anisotropy as described in Materials and Methods. The *K*_D values were obtained by fitting eq 4 to the data. ^dHydroxamate L161, 240 inhibition of LpxC activity was assessed at 30 °C [20 mM bis-tris propane, 10 mM TCEP (pH 7.5), and 1 mg/mL BSA] and 200 nM myr-UDP-GlcNAc as described in Materials and Methods. The IC₅₀ values were obtained by fitting eq 2 to the data. ^eData adapted from ref 18. ^fData adapted from ref 19.

that the higher activity and ligand affinity of Fe²⁺-EcLpxC correlate with the higher coordination number of Fe²⁺.

Effect of Fe²⁺ on Molecular Recognition. The metal ion status of LpxC was previously shown to influence the binding affinity of LpxC for small molecules, which has important implications for the development of LpxC inhibitors as potential antibiotics (18, 19). Here, we examine whether substitution of EcLpxC with Fe²⁺ alters the affinity of small molecules for LpxC compared to Zn²⁺ by measuring the affinities of myr-UDP-GlcNAc (*K*_D^{product}) and a fluorescent fatty acid (*K*_D^{fatty acid}) for LpxC (WT and C63A) using ultrafiltration and fluorescence anisotropy, respectively. The C63A mutation in LpxC causes a small enhancement in the binding affinity of these ligands, regardless of the metal ion at the active site (Table 4); the values of *K*_D^{product} and *K*_D^{fatty acid} are lowered 3–4- and < 2-fold, respectively, compared to that of WT LpxC. The value of *K*_D^{product} is not significantly altered when Fe²⁺- and Zn²⁺-EcLpxC are compared, in either WT or C63A, suggesting that product binding in these enzymes is similar and/or that there is not a direct metal ion–product interaction in these complexes. In contrast, an ~6-fold increase in *K*_D^{fatty acid} is observed for LpxC (WT and C63A) substituted with Fe²⁺ compared to that with Zn²⁺, indicating that changing the metal ion significantly alters the recognition of this small molecule, consistent with the direct metal ion–fatty acid interaction observed in crystal structures of the LpxC·palmitate complex (14, 32). Finally, a modest (2-fold) enhancement in inhibition (IC₅₀ value) by the hydroxamate inhibitor L-161,240 is observed for LpxC with bound Fe²⁺ compared to Zn²⁺ (Table 4). This is comparable to the 2-fold decrease in *K*_i for inhibition of histone deacetylase 8 by suberoylanilide hydroxamic acid upon switching the active site metal ion from Zn²⁺ to Fe²⁺ (11).

Oxygen Sensitivity of Fe²⁺-EcLpxC Activity. Since Fe²⁺ is a redox-sensitive metal ion, it is susceptible to oxidation. The initial rate of deacetylation catalyzed by LpxC after reconstitution with a stoichiometric amount of Fe²⁺ is decreased ≥ 8-fold when assayed under aerobic conditions compared to anaerobic conditions (glovebox). Furthermore, similar decreases were observed when the deacetylase activity of Fe²⁺-LpxC was measured in the presence of catalase (100 μg/mL), dithiothreitol (2 mM), dithionite (≤ 10 mM), or TCEP (≤ 2 mM) under aerobic conditions, suggesting that these conditions are not sufficient for maintaining

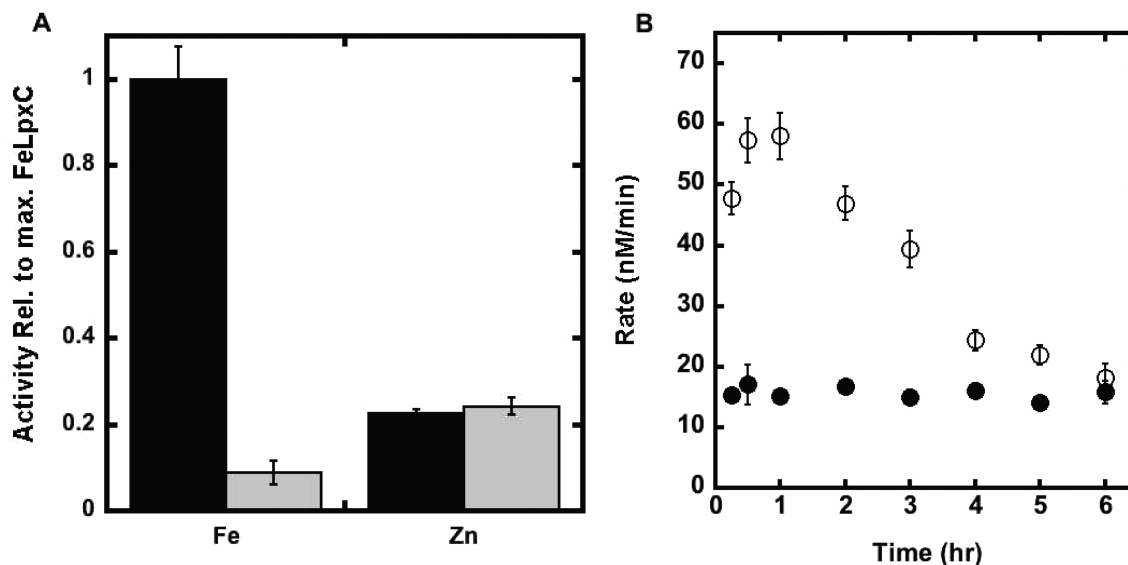


FIGURE 6: Dependence of LpxC activity on reducing agents. (A) The activity of Fe²⁺- and Zn²⁺-EcLpxC was measured at 30 °C in buffer containing either 10 mM TCEP (black bars) or 0.5 mM TCEP (gray bars) as described in Materials and Methods. (B) Apo-EcLpxC was reconstituted with either Fe²⁺ (○) or Zn²⁺ (●), and the resulting activity was measured at 30 °C [20 mM bis-tris propane and 10 mM TCEP (pH 7.5)] as a function of time.

Fe in the reduced form. However, when higher concentrations of TCEP (10 mM) are added to the assay, comparable deacetylase activity is observed for Fe²⁺-LpxC under both aerobic and anaerobic conditions over 2 h (Figure 6). In contrast, there is no change in Zn²⁺-LpxC activity when the concentration of TCEP is varied under these conditions (Figure 6A). Note that the activity of Fe²⁺-EcLpxC does not go to zero, but to the level observed for Zn²⁺-EcLpxC activity, suggesting that under these conditions the Fe²⁺ cofactor is replaced by nanomolar concentrations of adventitious Zn²⁺ in the assay. In vitro control experiments demonstrate that Fe²⁺-LpxC inactivated by exposure to oxygen can be reactivated by addition of divalent metal ions. These results demonstrate that the activity of Fe²⁺-LpxC, and not Zn²⁺-LpxC, is sensitive to exposure to oxygen.

Native LpxC Activity. To analyze the metal ion cofactor bound to LpxC in vivo, we measured the oxygen sensitivity of natively expressed LpxC in *E. coli* cell lysates. *E. coli* cells [BL21(DE3) without the LpxC expression plasmid] were grown and lysed, and the resulting LpxC activity was measured over time (from 15 min to 3 h following lysis) in buffers containing either ≤1 or 10 mM TCEP. The total native EcLpxC activity in cell lysates is ~3-fold higher in assays containing 10 mM TCEP compared to 0.1 mM TCEP (Figure 7, column A). Furthermore, over 3 h, the activity decreases ~5-fold (Figure 7, column B) to a residual activity that is stable in the cell lysate. If the residual activity measured in the presence of the LpxC hydroxamate inhibitor L-161,240 (Figure 7, column C), reflecting background deacetylation catalyzed by other enzymes, is subtracted from the oxygen-sensitive activity, then the observed activity decreases 5–7-fold in the presence of oxygen. This decrease is consistent with the higher activity of Fe²⁺-LpxC compared to that of Zn²⁺-LpxC. These findings suggest that the majority of the native LpxC expressed in *E. coli* contains a bound Fe²⁺ cofactor.

DISCUSSION

LpxC Activity Correlates with Metal Geometry. The kinetic experiments indicate that Fe²⁺ can serve as a cofactor for *E. coli* LpxC, a mononuclear metal-dependent deacetylase,

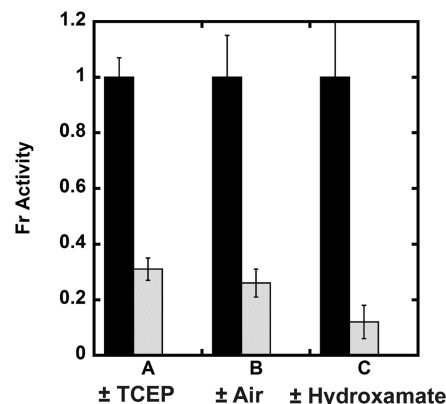


FIGURE 7: Native LpxC activity. The LpxC deacetylase activity of *E. coli* crude cell lysates was measured at 30 °C as described in Materials and Methods. (A) LpxC activity of *E. coli* cell lysate measured in 20 mM bis-tris propane (pH 7.5) containing 10 mM TCEP (black bars) or 0.1 mM TCEP (gray bars). (B) *E. coli* cell lysate activity assayed in 10 mM TCEP immediately following lysis (black bars) or after incubation on ice for 3 h under aerobic (benchtop) conditions postlysis (gray bars). (C) The LpxC inhibitor L-161,240 inhibits 90% of the deacetylase activity in the *E. coli* cell lysate [20 mM bis-tris propane and 10 mM TCEP (pH 7.5)]. The concentration of L-161,240 was 0 μM (black bars) or 1 μM (gray bars).

and that the Fe²⁺ cofactor alters the functional properties of LpxC compared to those of Zn²⁺. Specifically, LpxC substituted with a single catalytic Fe²⁺ has 6–8-fold higher activity than Zn²⁺-LpxC. Comparison of the steady-state kinetic parameters for the C63A mutant indicates that switching from Zn²⁺ to Fe²⁺ leads to a 6-fold increase in the value of k_{cat}/K_M , with a nearly comparable effect on the value of k_{cat} (4-fold). The single site mutation, C63A, eliminates much of the metal inhibition that complicates analysis of LpxC activity, likely by removing a ligand to the inhibitory metal.

Metal substitution in LpxC increases the value of both steady-state parameters k_{cat}/K_M and k_{cat} . The dependence of the value of k_{cat}/K_M for LpxC on the active site metal ion and on mutations (Table 1) (14, 18) argues that substrate association is not the rate-limiting step under these conditions even though the value of

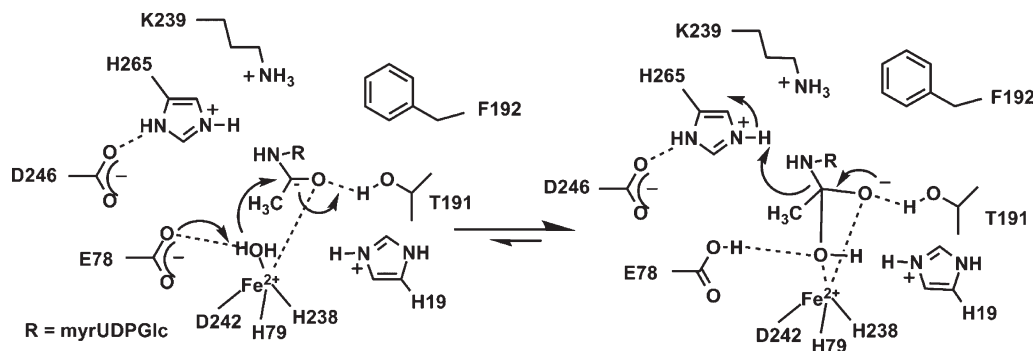


FIGURE 8: Proposed mechanism for EcLpxC.

k_{cat}/K_M [$\leq 1.6 \times 10^7 \text{ M}^{-1} \text{ s}^{-1}$ (Table 1)] approaches that of diffusion-controlled rate constants measured for many enzymes (10^7 – $10^8 \text{ M}^{-1} \text{ s}^{-1}$) (40). Additionally, the solvent kinetic isotope effect of 2 observed for k_{cat}/K_M catalyzed by LpxC (18) suggests that the chemical step is a rate-contributing step for this kinetic parameter. Additionally, under saturating substrate and high-enzyme concentration conditions, a burst of product formation is not observed, suggesting that the rate-limiting step in k_{cat} occurs at or before the chemical step (27). Therefore, it is reasonable to assume that the increases in k_{cat}/K_M and k_{cat} upon substitution of Zn^{2+} with Fe^{2+} are attributable mainly to an enhancement in the chemical step.

The best fit of the models to the XAS data includes five N or O ligands for both Fe^{2+} -substituted EcLpxC and AaLpxC compared to the four N or O ligands observed for WT Zn^{2+} -LpxC presumably due to an additional water ligand (12). These results are consistent with the hypothesis that the higher activity of the Fe^{2+} -substituted EcLpxC correlates with the coordination number. Previously, the enhanced activity of Fe^{2+} -peptide deformylase (PDF) has been proposed to be due, at least in part, to the higher coordination number of Fe^{2+} -PDF compared to that of Zn^{2+} -PDF (8, 28, 41–43). The XAS and activity data for Fe^{2+} -EcLpxC, in concert with recent crystallography data demonstrating a square pyramidal zinc site in LpxC in a complex with hydroxamate inhibitors or palmitate (26, 38), suggest that the proposed mechanism for deacetylation should be modified to incorporate a five-coordinate metal ion, in both the ground and transition states (Figure 8). In this mechanism, the metal ion serves both to lower the $\text{p}K_a$ of the metal-bound water and to coordinate the substrate (myr-UDP-GlcNAc). Coordination of the substrate to the metal ion can assist in polarization of the carbonyl group, enhancing the electrophilicity of the carbonyl carbon. However, enhancement of activity by the five-coordinate Fe^{2+} cofactor could also be due to small differences in metal–ligand bond length and ligand geometry that optimize the positions of the metal-bound water, the substrate carbonyl carbon, and active site side chains for catalyzing deacetylation. Following substrate binding, the side chain of E78 serves as a general base catalyst to activate the metal water for attack on the carbonyl carbon of the substrate (14, 27); the resulting oxanion intermediate is stabilized by the side chain of T191 and the metal ion (18). The mechanism that is most consistent with the crystallographic, theoretical studies and mutagenesis data (14, 18, 44) is one in which the side chain of protonated H265 [rather than protonated E78 as proposed for most metalloproteinases (45)] facilitates breakdown of the tetrahedral intermediate by protonation of the leaving group.

Molecular Recognition Is Affected by Metal Substitution. Previously, it has been demonstrated that apo-LpxC, LpxC

with a single bound zinc, and the zinc-inhibited form of LpxC (Zn_2 -LpxC) bind ligands with different affinities (19); similarly, switching the catalytic metal from Zn^{2+} to Fe^{2+} alters molecular recognition as well. The affinity of Fe^{2+} -EcLpxC for a hydroxamate inhibitor increases by a small degree (~ 2 -fold), consistent with crystal structures indicating that the metal geometry in LpxC-hydroxamate complexes is five-coordinate (square pyramidal) (26, 38). A similar increase in hydroxamate inhibitor affinity was observed when the active site metal was switched from Zn^{2+} to Fe^{2+} in histone deacetylase 8 (11). In addition, the affinity of Fe^{2+} -EcLpxC for the BODIPY-fatty acid inhibitor is decreased by 6-fold compared to that of the Zn-bound enzyme. Both changes in affinity are likely due to alteration of the geometry of the metal–ligand coordination, leading to alterations in interactions with other active site groups. Since the majority of LpxC inhibitors currently being developed as antibiotics interact with the active site metal ion, it is clear that the identity of this metal ion will affect the inhibitor efficacy.

Fe^{2+} -LpxC Is Redox-Sensitive in Vitro and Present in *E. coli*. Differences in the in vitro behaviors of Fe^{2+} -LpxC and Zn^{2+} -LpxC may provide information that will enable identification of the metal ion cofactor used by LpxC in vivo. In particular, the higher activity and oxygen sensitivity of Fe^{2+} -LpxC compared to those of Zn^{2+} -LpxC provide a means of evaluating the metal cofactor bound to LpxC in *E. coli* lysates. A majority of the native LpxC activity in *E. coli* cell lysates is lost upon exposure to oxygen (Figure 7). This suggests that *E. coli* grown aerobically in rich medium (LB) use Fe^{2+} as the main metal cofactor in LpxC and not Zn^{2+} . However, both Fe^{2+} and Zn^{2+} can activate LpxC-catalyzed deacetylation, and this metal switching capability may allow the LpxC to function, and *E. coli* to grow, under different environmental conditions, including limiting iron concentrations. Thus, LpxC likely fits into the category of a “cambialistic” enzyme that can be activated by either Fe or Zn, like several other enzymes, including the cambialistic Mn or Fe superoxide dismutases (46), metallo- β -lactamase L1 (47, 48), and the glyoxylases (49–51).

Given the effects of the active site metal bound to LpxC on turnover and molecular recognition, and the ongoing efforts to identify small-molecule inhibitors for this enzyme, most of which feature moieties that bind the catalytic metal ion, further experiments to determine the behavior and specificity of this enzyme in vivo are needed.

ACKNOWLEDGMENT

We gratefully acknowledge Ted Huston for ICP analysis, Chris Walsh for the gift of acyl carrier protein, Chris Raetz for the LpxA plasmid, and Michael Pirrung for the inhibitor

L-161,240. We also thank Rebekah Kelly for help with EXAFS analysis as well as Matthew Lattimer and the staff of Stanford Synchrotron Radiation Laboratory beamline 9-3.

REFERENCES

- Roth, L. D., Khan, A. S., Lillibridge, S. R., Ostroff, S. M., and Hughes, J. M. (2002) Public health assessment of potential biological terrorism agents. *Emerging Infect. Dis.* 8, 225–230.
- Raetz, C. R. H., and Whitfield, C. (2002) Lipopolysaccharide endotoxins. *Annu. Rev. Biochem.* 71, 635–700.
- Wyckoff, T. J. O., Raetz, C. R. H., and Jackman, J. E. (1998) Antibacterial and anti-inflammatory agents that target endotoxin. *Trends Microbiol.* 6, 154–159.
- White, R. J., Margolis, P. S., Trias, J., and Yuan, Z. Y. (2003) Targeting metalloenzymes: A strategy that works. *Curr. Opin. Pharmacol.* 3, 502–507.
- Young, K., Silver, L. L., Bramhill, D., Cameron, P., Eveland, S. S., Raetz, C. R. H., Hyland, S. A., and Anderson, M. S. (1995) The envA permeability cell division gene of *Escherichia coli* encodes the second enzyme of lipid A biosynthesis: UDP-3-O-(R-3-hydroxymyristoyl)-N-acetylglucosamine deacetylase. *J. Biol. Chem.* 270, 30384–30391.
- Jackman, J. E., Raetz, C. R. H., and Fierke, C. A. (1999) UDP-3-O-(R-3-hydroxymyristoyl)-N-acetylglucosamine deacetylase of *Escherichia coli* is a zinc metalloenzyme. *Biochemistry* 38, 1902–1911.
- Groche, D., Becker, A., Schlichting, I., Kabsch, W., Schultz, S., and Wagner, A. F. V. (1998) Isolation and crystallization of functionally competent *Escherichia coli* peptide deformylase forms containing either iron or nickel in the active site. *Biochem. Biophys. Res. Commun.* 246, 342–346.
- Rajagopalan, P. T. R., Yu, X. C., and Pei, D. H. (1997) Peptide deformylase: A new type of mononuclear iron protein. *J. Am. Chem. Soc.* 119, 12418–12419.
- Becker, A., Schlichting, I., Kabsch, W., Groche, D., Schultz, S., and Wagner, A. F. V. (1998) Iron center, substrate recognition and mechanism of peptide deformylase. *Nat. Struct. Biol.* 5, 1053–1058.
- Zhu, J. G., Dizin, E., Hu, X. B., Wavreille, A. S., Park, J., and Pei, D. H. (2003) S-Ribosylhomocysteine (LuxS) is a mononuclear iron protein. *Biochemistry* 42, 4717–4726.
- Gantt, S. L., Gattis, S. G., and Fierke, C. A. (2006) Catalytic activity and inhibition of human histone deacetylase 8 is dependent on the identity of the active site metal ion. *Biochemistry* 45, 6170–6178.
- McClure, C. P., Rusche, K. M., Peariso, K., Jackman, J. E., Fierke, C. A., and Penner-Hahn, J. E. (2003) EXAFS studies of the zinc sites of UDP-(3-O-acyl)-N-acetylglucosamine deacetylase (LpxC). *J. Inorg. Biochem.* 94, 78–85.
- Jackman, J. E., Fierke, C. A., Tumey, L. N., Pirrung, M., Uchiyama, T., Tahir, S. H., Hinds, O., and Raetz, C. R. H. (2000) Antibacterial agents that target lipid A biosynthesis in Gram-negative bacteria: Inhibition of diverse UDP-3-O-(R-3-hydroxymyristoyl)-N-acetylglucosamine deacetylases by substrate analogs containing zinc binding motifs. *J. Biol. Chem.* 275, 11002–11009.
- Hernick, M., Gennadios, H. A., Whittington, D. A., Rusche, K. M., Christianson, D. W., and Fierke, C. A. (2005) UDP-3-O-(R-3-hydroxymyristoyl)-N-acetylglucosamine deacetylase functions through a general acid-base catalyst pair mechanism. *J. Biol. Chem.* 280, 16969–16978.
- Sorensen, P. G., Lutkenhaus, J., Young, K., Eveland, S. S., Anderson, M. S., and Raetz, C. R. H. (1996) Regulation of UDP-3-O-R-3-hydroxymyristoyl-N-acetylglucosamine deacetylase in *Escherichia coli*. The second enzymatic step of lipid A biosynthesis. *J. Biol. Chem.* 271, 25898–25905.
- Onishi, H. R., Pelak, B. A., Gerckens, L. S., Silver, L. L., Kahan, F. M., Chen, M. H., Patchett, A. A., Galloway, S. M., Hyland, S. A., Anderson, M. S., and Raetz, C. R. H. (1996) Antibacterial agents that inhibit lipid A biosynthesis. *Science* 274, 980–982.
- Jackman, J. E., Raetz, C. R., and Fierke, C. A. (1999) UDP-3-O-(R-3-hydroxymyristoyl)-N-acetylglucosamine deacetylase of *Escherichia coli* is a zinc metalloenzyme. *Biochemistry* 38, 1902–1911.
- Hernick, M., and Fierke, C. A. (2006) Catalytic Mechanism and Molecular Recognition of *E. coli* UDP-3-O-(R-3-Hydroxymyristoyl)-N-acetylglucosamine Deacetylase Probed by Mutagenesis. *Biochemistry* 45, 15240–15248.
- Hernick, M., and Fierke, C. A. (2006) Molecular recognition by *Escherichia coli* UDP-3-O-(R-3-hydroxymyristoyl)-N-acetylglucosamine deacetylase is modulated by bound metal ions. *Biochemistry* 45, 14573–14581.
- George, G. N. <http://www-ssrl.slac.stanford.edu/exafspak.html>.
- Ankudinov, A. L., and Rehr, J. J. (1997) Relativistic calculations of spin-dependent X-ray-absorption spectra. *Phys. Rev. B* 56, R1712–R1715.
- Ankudinov, A. L., Ravel, B., Rehr, J. J., and Conradson, S. D. (1998) Real-space multiple-scattering calculation and interpretation of X-ray-absorption near-edge structure. *Phys. Rev. B* 58, 7565–7576.
- McMaster, W. H., Del Grande, J. H., Mallet, N. K., and Hubbell, J. H. (1969) Compilation of X-Ray Cross Sections. Lawrence Livermore National Laboratory Report UCRL-50174, Section II, Revision 1, National Institute of Standards and Technology, Gaithersburg, MD.
- Weng, T. C., Waldo, G. S., and Penner-Hahn, J. E. (2005) A method for normalization of X-ray absorption spectra. *J. Synchrotron Radiat.* 12, 506–510.
- Irving, H., and Williams, R. J. P. (1948) Order of Stability of Metal Complexes. *Nature* 162, 746–747.
- Whittington, D. A., Rusche, K. M., Shin, H., Fierke, C. A., and Christianson, D. W. (2003) Crystal structure of LpxC, a zinc-dependent deacetylase essential for endotoxin biosynthesis. *Proc. Natl. Acad. Sci. U.S.A.* 100, 8146–8150.
- McClarren, A. L., Zhou, P., Guan, Z., Raetz, C. R. H., and Rudolph, J. (2005) Kinetic Analysis of the Zinc-Dependent Deacetylase in the Lipid A Biosynthetic Pathway. *Biochemistry* 44, 1106–1113.
- Jain, R. K., Hao, B., Liu, R. P., and Chan, M. K. (2005) Structures of *E. coli* peptide deformylase bound to formate: Insight into the preference for Fe²⁺ over Zn²⁺ as the active site metal. *J. Am. Chem. Soc.* 127, 4558–4559.
- Lippard, S. J., and Berg, J. M. (1994) Principles of Bioinorganic Chemistry, University Science Books, Mill Valley, CA.
- Frausto da Silva, J. J. R., and Williams, R. J. P. (2001) The Biological Chemistry of the Elements, Oxford University Press, New York.
- Kaim, W., and Schwederski, B. (1994) Bioinorganic Chemistry: Inorganic Elements in the Chemistry of Life, John Wiley and Sons Ltd., Chichester, U.K.
- Gennadios, H. A., and Christianson, D. W. (2006) Binding of uridine 5'-diphosphate in the "basic patch" of the zinc deacetylase LpxC and implications for substrate binding. *Biochemistry* 45, 15216–15223.
- Shu, L., Chiou, Y. M., Orville, A. M., Miller, M. A., Lipscomb, J. D., and Que, L., Jr. (1995) X-ray absorption spectroscopic studies of the Fe(II) active site of catechol 2,3-dioxygenase. Implications for the extradiol cleavage mechanism. *Biochemistry* 34, 6649–6659.
- Westre, T. E., Kennepohl, P., DeWitt, J. G., Hedman, B., Hodgson, K. O., and Solomon, E. I. (1997) A multiplet analysis of Fe K-edge 1s → 3d pre-edge features of iron complexes. *J. Am. Chem. Soc.* 119, 6297–6314.
- Roe, A. L., Schneider, D. J., Mayer, R. J., Pyrz, J. W., Widom, J., and Que, L. (1984) X-ray Absorption-Spectroscopy of Iron-Tyrosinate Proteins. *J. Am. Chem. Soc.* 106, 1676–1681.
- Thorpe, H. H. (1992) Bond Valence Sum Analysis of Metal-Ligand Bond Lengths in Metalloenzymes and Model Complexes. *Inorg. Chem.* 31, 1585–1588.
- Brown, I. D., and Altermatt, D. (1985) Bond-Valence Parameters Obtained from a Systematic Analysis of the Inorganic Crystal-Structure Database. *Acta Crystallogr.* B41, 244–247.
- Mochalkin, I., Knafels, J. D., and Lightle, S. (2008) Crystal structure of LpxC from *Pseudomonas aeruginosa* complexed with the potent BB-78485 inhibitor. *Protein Sci.* 17, 450–457.
- Hakansson, K., Wehnert, A., and Liljas, A. (1994) X-ray Analysis of Metal-Substituted Human Carbonic-Anhydrase-II Derivatives. *Acta Crystallogr.* D50, 93–100.
- Fersht, A. R. (1999) Structure and Mechanism in Protein Science: A Guide to Enzyme Catalysis and Protein Folding, W. H. Freeman and Co., New York.
- Rajagopalan, P. T., Datta, A., and Pei, D. (1997) Purification, characterization, and inhibition of peptide deformylase from *Escherichia coli*. *Biochemistry* 36, 13910–13918.
- Rajagopalan, P. T., and Pei, D. (1998) Oxygen-mediated inactivation of peptide deformylase. *J. Biol. Chem.* 273, 22305–22310.
- Chan, M. K., Gong, W., Rajagopalan, P. T., Hao, B., Tsai, C. M., and Pei, D. (1997) Crystal structure of the *Escherichia coli* peptide deformylase. *Biochemistry* 36, 13904–13909.
- Robinet, J. J., and Gaud, J. W. (2008) DFT investigation on the mechanism of the deacetylation reaction catalyzed by LpxC. *J. Phys. Chem. B* 112, 3462–3469.
- Christianson, D. W., and Cox, J. D. (1999) Catalysis by metal-activated hydroxide in zinc and manganese metalloenzymes. *Annu. Rev. Biochem.* 68, 33–57.
- Martin, M. E., Byers, B. R., Olson, M. O. J., Salin, M. L., Arceneaux, J. E. L., and Tolbert, C. (1986) A *Streptococcus mutans* Superoxide Dismutase That Is Active with Either Manganese or Iron as a Cofactor. *J. Biol. Chem.* 261, 9361–9367.

47. Hu, Z., Spadafora, L. J., Hajdin, C. E., Bennett, B., and Crowder, M. W. (2009) Structure and Mechanism of Copper- and Nickel-Substituted Analogues of Metallo- β -lactamase L1 (dagger). *Biochemistry* 48, 2981–2989.
48. Hu, Z. X., Gunasekera, T. S., Spadafora, L., Bennett, B., and Crowder, M. W. (2008) Metal content of metallo- β -lactamase L1 is determined by the bioavailability of metal ions. *Biochemistry* 47, 7947–7953.
49. Limphong, P., McKinney, R. M., Adams, N. E., Makaroff, C. A., Bennett, B., and Crowder, M. W. (2010) The metal ion requirements of *Arabidopsis thaliana* Glx2-2 for catalytic activity. *J. Biol. Inorg. Chem.* 2, 249–258.
50. Limphong, P., Nimako, G., Thomas, P. W., Fast, W., Makaroff, C. A., and Crowder, M. W. (2009) *Arabidopsis thaliana* Mitochondrial Glyoxalase 2-1 Exhibits β -Lactamase Activity. *Biochemistry* 48, 8491–8493.
51. Limphong, P., McKinney, R. M., Adams, N. E., Bennett, B., Makaroff, C. A., Gunasekera, T., and Crowder, M. W. (2009) Human Glyoxalase II Contains an Fe(II)Zn(II) Center but Is Active as a Mononuclear Zn(II) Enzyme. *Biochemistry* 48, 5426–5434.